Impact of the Convection Triggering Function on the Single-Column Model Simulations

Shaocheng Xie and Minghua Zhang

Institute for Terrestrial and Planetary Atmosphere, State University of New York at Stony Brook, Stony Brook, New York

Corresponding author address: Dr. Shaocheng Xie, L-103, ASD, Lawrence Livermore National Laboratory, Livermore, CA 94550

Abstract. We analyze the causes of the large thermal biases in the simulation of the NCAR CCM3 Single-Column Model (SCM) when it is forced with the Atmospheric Radiation Measurement Program's (ARM) summer 1995 Intensive Observing Period (IOP) data. We have found that deficiencies of the convection triggering function used in the model can explain a significant part of the biases. In the model, convection is triggered whenever there is positive convective available potential energy (CAPE), which happens to occur during daytime due to solar heating of the land surface. In observations, however, convection takes place only when the large-scale dynamic condition is favorable to the release of CAPE. Based on observations, we propose a new triggering function for the CCM3 deep convection scheme. We assume that model convection occurs only when the large-scale dynamic forcing makes positive contributions to the existing positive CAPE. Improved simulation results are obtained when the new triggering function is implemented in the model. We further test the new triggering function using the ARM SGP summer 1997 IOP data and the Global Atmospheric Research Program's Atlantic Tropical Experiment (GATE) phase III observations. These tests confirm the results obtained from the ARM 1995 experiments.

1. Introduction

A Single-Column Model (SCM) represents a grid column of a general circulation model (GCM). By specifying the large-scale advective tendencies, an SCM can be used effectively to test the performance of the GCM parameterizations [*Lord*, 1982; *Kuo and Anthes*, 1984; *Betts and Miller*, 1986; *Grell et al.*, 1991; *Xu and Arakawa*, 1992; *Randall et al.*, 1996]. Recently, several problems have emerged with the use of the SCM approach [*Ghan et al.*, 1999; *Hack and Pedretti*, 1999]. One of them is that model solutions, such as the predicted temperature and moisture fields, can drift away from observations after a few days of integration. This is mainly due to the absence of effective internal feedback between the SCM and the large-scale dynamic input. Large biases in model simulations prevent meaningful evaluations of the GCM parameterizations. These biases are caused by the combination of inaccurate input data and deficient model parameterizations.

One of the required efforts is therefore to improve the quality of the large-scale forcing data. Forcing data derived from previous objective analysis [e.g., *Barnes*, 1964; *O'brien*, 1970; *Lin and Johnson*, 1996] may contain large errors. For example, objectively analyzed field data typically do not conserve column-integrated heat, moisture, and momentum. The unbalanced budgets can cause serious problems in SCMs [*Zhang and Lin*, 1997]. To reduce these problems, *Zhang and Lin* [1997] proposed a constrained variational analysis approach, in which the atmospheric state variables are forced to satisfy the conservation of mass, heat, moisture, and momentum through a variational technique. This method has been applied to process the observational data collected from the ARM program. Results from an SCM intercomparison study have shown improved performance of SCMs [*Ghan et al.*, 1999].

As a parallel effort to address the large SCM simulation biases, this paper attempts to reveal and reduce deficiencies in the model physical parameterizations. The NCAR CCM3 SCM is used in this study, with forcing data collected from the Southern Great Plain (SGP)

Cloud and Radiation Testbed (CART) site of the ARM program for the summer 1995 IOP. Simulation results show large warm biases in temperature of up to 20 K. After detailed analysis, we identified that the triggering function used in the CCM3 deep convection scheme (ZM, hereafter) [*Zhang and McFarlane*, 1995] is one main cause for the large temperature biases. It is shown that occurrence of CAPE is not a sufficient condition to trigger convection, which is assumed in the ZM scheme. Based on the observations, a new triggering function is proposed to account for the dynamical influences of circulation on the initiation of convection. The new triggering function and simulation results are discussed in the paper. We further use the ARM summer 1997 IOP data and the GATE phase III observations to show the performance of the new triggering function in other SCM cases and climate regions.

2. Model and data

2.1. The CCM3 SCM

The SCM used in this study was developed from the CCM3 by the NCAR SCM group (courtesy of Dr. James Hack) [*Hack et. al.*, 1998]. Physical parameterizations in the SCM are the same as those in the CCM3. They include the parameterization of clouds, radiation, deep and shallow moist convection, large-scale condensation, vertical diffusion, and atmospheric boundary processes. Detailed description about these components can be found in *Kiehl et al.* [1996].

The thermodynamic and moisture equations in the CCM3 SCM are

$$\frac{\partial T}{\partial t} = T_{HLS} - \omega(\frac{\partial T}{\partial p} + \frac{RT}{pc_p}) + T_{phy} \tag{1}$$

$$\frac{\partial q}{\partial t} = q_{HLS} - \omega\frac{\partial q}{\partial p} + q_{phy} \tag{2}$$

where T, q and ω are the temperature, mixing ratio of water vapor, and vertical velocity, respectively. The terms T_{HLS} and q_{HLS} represent the large-scale horizontal advective forcing

terms. c_P is the specific heat at constant pressure. The terms T_{phy} and q_{phy} represent the collection of parameterized physics terms.

The standard model configuration of the CCM3 SCM is used in the experiments, in which the horizontal advective tendencies of temperature (T_{HLS}) and moisture (q_{HLS}) are specified from observations and the vertical advective tendencies are calculated by using the observed vertical velocity and predicted temperature and water vapor mixing ratio profiles in the SCM. For the vertical advection, the CCM semi-Lagrangian procedure [*Williamson and Rasch*, 1994] is used to advect water vapor mixing ratio and the CCM 2nd-order Eulerian finite-difference scheme [*Williamson*, 1988] is used to advect temperature. Surface fluxes and ground temperature are calculated from the CCM3 land surface model.

2.2. Data

The data used to force and validate the SCM is obtained from the ARM July 1995 IOP observations around the CART facility at SGP. The horizontal advective tendencies of temperature and moisture, and the vertical velocity, are derived from the variational analysis of *Zhang and Lin* [1997]. This IOP starts from 18 July (0530Z) 1995 and ends on 4 August (0530Z) 1995. It experienced a wide range of summertime weather conditions. It includes several intensive precipitation events every other day associated with a stationary, large-scale upper-level trough over North America in the first half of the period, and then followed by a few clear days associated with an upper-level ridge. In the end of the period, a strong upper-level trough moved into the SGP, with increasing cloudiness, thunderstorms, and continuous precipitation. The observed precipitation and the large-scale advective tendencies of temperature and moisture are shown in Figure 1. Corresponding to the precipitation periods, strong dynamic cooling (associated with upward motion) is seen in the middle and upper troposphere, and large-scale moisture convergence is noted in the lower levels. On day 12, there are quite large cooling and moisten but there is no surface precipitation observed. This is probably because the

condensed water is re-evaporated before it reaches the surface. In other periods, downward motions prevail. Therefore, this period provides a variety of weather conditions to evaluate the performance of the SCM.

3. Analysis of Results

3.1. Simulation Results

Studies from *Cripe* [1998] and *Hack and Pedretti* [1999] have shown that the SCM solutions are sensitive to initial conditions because of the non-linear nature of model physics. *Hack and Pedretti* [1999] further showed that a single model solution is not of representative and an ensemble methodology is needed. In this study, we conduct a set of 100 ensemble runs using the same forcing, but slightly different initial conditions for temperature and water vapor mixing ratio. Similar to *Hack and Pedretti* [1999], perturbations in temperature and water vapor mixing ratio fields are randomly generated, characterized by a standard deviation of 0.5 K for temperature and a maximum standard deviation of 0.5 g/Kg, for water vapor mixing ratio in the atmospheric boundary layer. The perturbations are bounded by 1 K and 6% of the locally observed water vapor mixing ratio.

Differences between the ensemble mean of simulated temperature and moisture and the observations are shown in Figures 2a and 2b, respectively. It is seen that the model produces large warm biases after day 8 (Figure 2a). The warm biases extend to all model layers with one maximum center located around 400 mb on day 10 and the other two in the lower troposphere on day 9 and day 13-14, respectively. For the moisture field (Figure 2b), the model generally produces dry biases in the lower troposphere. To determine whether or not these errors are statistically significant, we show in Figure 2c the standard deviations of the ensemble mean temperature biases.   It is seen that the model does show sensitivity to initial conditions to a certain degree. The large standard deviations of temperature errors in the lower troposphere are associated with interactions between cumulus convection and atmospheric boundary layer processes [*Hack and Pedretti*, 1999].   We note that the

standard deviations are rather small in the region where large warm biases occur, suggesting that the warm biases produced by the model are physically significant. The moisture field exhibits similar sensitivity to initial conditions as seen in the temperature field.

Figure 3 shows the ensemble mean of simulated precipitation rates (dotted line) and the standard deviations (dash dotted line). In comparison with the observed precipitation (solid line), the model generates too often and too weak precipitation with significant phase shift in its peaks. The simulated precipitation shows a strong diurnal variation, with overestimation during the day and underestimation during the night. Here, local noon corresponds to GMT 17:00 pm in the figure. The standard deviations are generally much smaller than the predicted precipitation. The features in Figure 3 suggest possible deficiencies in the triggering functions of the CCM3 deep convection scheme.

Figures 4a and 4b show the time-pressure cross section of the observed and simulated ensemble mean apparent heat sources (Q1), respectively. The definition of Q1 can be found in *Yanai et al.* [1973]. Compared with the observed Q1, the model produces excess heating during the day and less heating during the night (see days 2, 4, 6, and 8 - 9 in Figure 4b), which is consistent with the phase problem in its predicted precipitation rates. These effects offset each other to some extent in the first few days (from day 1 to day 8), thereby giving relatively small errors in the temperature simulation in this period. The offsetting does not have any physical meanings. Instead, it hides problems in the parameterization. On days 9 and 10, the model produces large spurious heatings during the daytime, rather than the observed coolings, thereby leading to the largest warm biases at 400 mb around days 9-11.

The above discussion suggests that the simulation errors may be closely related to model cumulus convection. Deficiencies in convective triggering function could be one of the reasons responsible for the large model biases.

3.2. Analysis and experiments with the convection triggering function

The deep convection scheme used in the CCM3 is proposed by *Zhang and McFarlane* [1995]. It is based on the plume ensemble concept similar to *Arkawa and Schubert* [1974]. The scheme assumes that convection occurs whenever there is positive CAPE. This assumption has obvious weakness. For instance, observations from the GATE showed a negative correlation between CAPE and convective activities [*Thompson et al.*, 1979]. *Wang and Randall* [1994] showed that CAPE accumulated before convection began during the GATE phase III period. In nature, the accumulation of large reservoirs of CAPE is a prerequisite for strong convection. For a conditionally unstable sounding, its thermodynamic structure often shows an appreciable depth of negative buoyancy (usually referred to as convection inhibition) below the level of free convection [*Fritsch and Kain*, 1993; *Emanuel*, 1994]. Convective instability cannot be released spontaneously unless an external source of energy is supplied to the air mass to overcome the amount of convection inhibition so that it can rise to the level of free convection. The existence of CAPE can only be considered as a necessary condition for convection, but not a sufficient condition.

The relationship between CAPE and strong convection in the ARM observations is illustrated in Figure 5, which shows the time series of total CAPE from the surface to the neutral buoyancy level, total negative CAPE (NCAPE, hereafter), and precipitation. We use precipitation as a proxy of cumulus convective activities. CAPE is calculated under the assumption that an air parcel ascends along a reversible moist adiabat with the level of origin at the surface:

$$CAPE = R_d \int_{P_n}^{P_i} (T_{vp} - T_v)\, d\ln p \qquad (3)$$

and negative CAPE is defined as:

$$NCAPE = R_d \int_{p_f}^{P_i} (T_{vp} - T_v)\, d\ln p \qquad (4)$$

where p_n is the neutral buoyancy pressure for an air parcel originating from p_i and p_f is the pressure at the level of free convection. T_{vp} is the virtual temperature of the parcel, and T_v is the virtual temperature of the ambient air at the same level.

Consistent with other studies, Figure 5 shows that the existence of CAPE does not guarantee the onset of convection. For instance, even though large CAPE exists in the atmosphere during day 9 to day 13, no convective activities are observed. The CAPE exhibits strong diurnal variations with maximum during the day and minimum during the night due to the strong solar diurnal cycle over the land surface. Furthermore, the negative CAPE is relatively large at night when convection actually occurs. As a consequence, the triggering condition of the ZM scheme, which relies on positive CAPE, results in overestimation of convection during the day and underestimation of convection during the night. As can be seen, in the observations, most of the convective events occur during the night in this IOP. This feature cannot be captured by the model. Therefore, it is not surprising that there are obvious phase shifts between the simulated precipitation and the observed precipitation (Figure 3). Since CAPE cannot accumulate in the model, the simulated intensity of convective precipitation is also weaker than that in the observations.

The above discussion demonstrates that additional favorable conditions are needed to initiate convection. It is well known that the large-scale dynamic forcing (e.g., large-scale low-level convergence) plays an important role in destabilizing the atmospheric structure, initiating and maintaining deep cumulus convection. It appears necessary to link the convective triggering condition to these large-scale dynamic processes. In fact, many efforts have been made in the past. *Kuo* [1965 and 1974] requires the large-scale moisture convergence in his convection scheme to prevent conditional instability from being released spontaneously. *Fritsch and Chappell* [1980], *Kain and Fritsch* [1993], and *Rogers and Fritsch* [1996] link convective triggering condition to the amount of inhibition that must be overcome before convection can be initiated. In their schemes, the perturbations of temperature and vertical velocity are parameterized in terms of the large-

scale low-level convergence. The triggering functions in their schemes may help avoid excessive convection in area where the low-level upward motion is weak.

This paper proposes a new triggering function for the ZM scheme. We use a dynamic CAPE production rate (DCAPE, hereafter), similar to that used in the study *of Wang and Randall* [1994], to incorporate the dynamic processes. DCAPE is defined as the difference of CAPE between a hypothetical atmospheric state, which is the observed sounding plus the change due to the total large-scale advection over a time interval Δt, and the observed state. It should be pointed out that the definition of our hypothetical state is different from that defined in *Wang and Randall* [1994]. They defined it as a state modified by the effects of all non-convective processes, including the total large-scale advection, radiation, and surface fluxes of the sensible and latent heat. Our purpose here is to reduce the effect of solar diurnal cycle on the initiation of convection. Solar radiation and surface fluxes are considered to contribute to build up CAPE, but not to trigger the release of CAPE. Therefore, the DCAPE, in this paper, is solely due to the joint impact of upward motion and horizontal advections of temperature and moisture.

Figure 6 shows the observed relationship between the positive DCAPE and the convective events. It is seen that cumulus convection is closely related to the large-scale dynamic processes. The strong diurnal variation in the CAPE shown in Figure 5 is not present in the positive DCAPE. Using the positive DCAPE as an index for the onset of convection not only links the convective activities with atmospheric dynamic processes, but also reduces the control of the solar diurnal cycle on the initiation of convection. Based on this feature, we made a simple modification to the ZM convection scheme. We assume that model convection occurs only when the large-scale advection, including horizontal and vertical advection, makes a positive contribution to the existing positive CAPE. It should be emphasized that this assumption differs in its nature with the Kuo-type schemes in that moisture convergence is not used as a closure of the scheme.

We note that the radiative and surface processes can also destabilize atmosphere and induce cumulus convection. Without the support of large-scale dynamic processes, however, convections that are solely induced by radiation and surface fluxes are likely to be shallow, which fall into the category of convective boundary layer and should not be treated as deep convection.

In our actual implementation, to avoid the impact of computational noises in the calculated DCAPE, we require DCAPE to be larger than a threshold value (100 J/kg/hr is used in current experiment), which is usually one order of magnitude smaller than those observed in strong convective systems. When DCAPE is less than this threshold value but larger than zero, we reduce the cloud base mass flux. We simply assume that the reduction factor has a linear relationship with the positive DCAPE. This reduction is equivalent to extending the convective adjustment time scale (τ_{adj}) when the large-scale dynamic forcing is weak (small positive DCAPE). It is consistent with *Wang and Randall* [1996], who found that τ_{adj} is related to the rate of change of the generalized convective available potential energy (GCAPE) by large-scale processes, including horizontal and vertical advections of temperature and moisture and radiation. Larger GCAPE production rate corresponds to smaller values of τ_{adj}, while smaller GCAPE production rate corresponds to larger values of τ_{adj}.

Figure 7 shows the simulated precipitation rates using the modified ZM scheme (ZM_m, hereafter). The figure shows significant improvements in both the phase and magnitude of the simulated precipitation compared with Figure 3. The standard deviations are small in the strong precipitation periods. Consistent with the precipitation rates, improvements are found in the simulated Q1 field (Figure 8). The spurious heating estimated from the ZM scheme on day 9 is largely reduced in the ZM_m scheme. As a result, simulations of the temperature and moisture are obviously improved (Figure 9a and 9b). It is seen that both the area and magnitude of the warm biases in Figure 2a are significantly reduced in Figure 9a. The large dry biases shown in Figure 2b are also

reduced in Figure 9b.   Figure 9b shows slightly moist biases. It is also noted that the modified scheme produces smaller standard deviations of the ensemble mean temperature errors than the original version. The large standard deviations near the surface in Figure 2c are largely reduced in Figure 9c. This indicates that the improved scheme also reduces the model sensitivity to initial conditions.

3.3. Experiments with the ARM 1997 IOP and GATE observations

   The robustness of the above results is further testes using the recently available summer 1997 IOP data collected at the ARM SGP site and the GATE phase III observations over the tropical Atlantic ocean. For simplicity, in this part, we will only show results from the model standard run.

(a) ARM 1997 simulations

   The data used in the experiment is processed exactly the same as those used in the ARM 1995 simulations. It covers the period from 2330Z 18 June 1997 to 2330Z 17 July 1997. This is also a convectively driven period. Several intensive convective precipitation events were observed during this IOP (see the solid line in Figure 10).

   Figure 10 (a) and (b) show the time series of the observed and simulated precipitation rates from the ZM scheme and the ZM_m scheme, respectively. Similar to the experiments with the ARM 1995 IOP data, the ZM scheme produces excessive precipitation almost every day during the daytime.   Its precipitation shows strong diurnal variation.   This problem is significantly reduced in the ZM_m scheme, which generally well captures the observed precipitation.

   Figure 11 shows the time-pressure cross section of the simulated and observed Q1. Similar to the ARM 95 experiments, the heating produces by the ZM scheme shows obvious phase bias compared with the observed Q1.   It overestimates the heating during the day and underestimates the heating during the night.   In general, the heating is

overestimated below 200 mb and underestimated above. In comparison with the ZM scheme, the simulated Q1 from the ZM_m scheme is much closer to the observed Q1. The position of the heating maxima is generally well captured, although it fails to reproduce the heating as strong as observed, especially in the upper troposphere.

Figures 12 and 13 show the temperature and moisture biases for these two schemes, respectively. It is seen that large warm and dry biases produced by the ZM scheme (Figures 12(a) and 13(a)) are significant reduced by the ZM_m scheme (Figures 12(b) and 13(b)). This indicates that the problem in the triggering function of the ZM scheme is again one of the main reasons for these biases. In Figure 12 (b), the ZM_m scheme shows cold biases (less than 10 K) in the middle and upper troposphere, which are related to the underestimation of Q1 as discussed before.

(b) GATE simulations

The GATE phase III observations cover the period from 00Z 30 August to 24Z 18 September 1974. During this period, the atmosphere experienced robust convective events. The GATE data have been widely used for studying interactions between cumulus convection and large-scale circulation and for validating cumulus convection schemes in the past. We use these data here to further test the validity of the proposed triggering function over the tropical ocean. In this experiment, the forcing is specified in the same way as the ARM experiment and integration covers the period from 00Z 1 September to 24Z 17 September 1974.

The GATE data are originally obtained from the Colorado State University (CSU) SCM group. They are on the 1 x 1 degree square grid box, covering an area of 9 x 9 degree squares within 4 N – 14 N, 19 W – 28 W, with 19 layers from 991.25 mb to 92.56 mb. The frequency of the GATE observations is 3 hours. The forcing data used to drive the CCM3 SCM are averaged over the innermost 9 grids, and then cubic interpolated onto 20-minute intervals. These forcing data are constructed and provided by the NCAR SCM group.

Figure 14 compares the simulated precipitation (dotted line) with the "observed" precipitation (solid line). The "observed" precipitation in the figure is obtained through vertically integrating the observed apparent moisture sinks (Q2), which is defined in *Yanai et al.* (1973). It is seen that the ZM scheme slightly lags the "observed" precipitation in almost all precipitation peaks, and the peaks of the "observed" precipitation on days 13-14 are significantly underestimated (Figure 14 (a)). These biases are reduced by the ZM_m scheme. In particular, this scheme well reproduces the "observed" precipitation on days 13-14 (Figure 14 (b)).

Figure 15 shows the calculated and observed Q1 for the GATE experiment. As compared with the observations, the ZM_m scheme gives a much better simulation of the Q1 than the ZM scheme. For example, the ZM scheme fails to reproduce the strong heating observed on day 13, while it is well captured by the ZM_m scheme.

Figures 16 and 17 show the temperature and moisture biases, respectively. The biases in the simulated temperature and moisture for these two schemes are much smaller than those in the ARM experiments, except for the large warm biases produced in the upper troposphere (above 200 mb). These warm biases are probably due to the extrapolation of the input data onto the uppermost four model levels, which are beyond the observation range. Compared with the ZM scheme, the ZM_m scheme improves the simulations in both the temperature and moisture fields. The large cold biases on days 14 – 17 and dry biases on days 9 – 15 produced by the ZM scheme (Figure 16 (a) and 17 (a)) are largely reduced by the ZM_m scheme (Figure 16(b) and 17(b)).

4. Summary and discussion

With input data from the ARM 1995 summer IOP, we have shown that the NCAR CCM3 SCM with the ZM scheme produces large warm biases. The triggering function in the ZM scheme is analyzed to compare with observations. It is identified as one of the major causes for the simulation biases. The strong solar diurnal heating controls the

generation and variation of convective available potential energy, which leads the ZM scheme to overestimate convection during the day and underestimate it during the night.

Many studies have pointed out that CAPE is a necessary but not a sufficient condition for initiating convection. A strong relationship between the positive dynamic generation rate of the CAPE (DCAPE) and deep convection is found in the observations. The relationship implies that large-scale dynamic processes are necessary to disturb and lift air parcel to its level of free convection. Based on the relationship, we enforced an additional requirement of positive DCAPE to initiate convection in the ZM convection scheme. Significant improvements in the simulation of temperature are obtained when the new modified convection scheme is used.

The results from the ARM 1995 experiment are further confirmed in the ARM 1997 experiment. We note that the problem of the triggering function in the ZM scheme in the GATE experiment is not as serious as in the ARM experiments because of the weaker solar diurnal cycle over the tropical ocean. However, the modified scheme still gave much better simulation results than the original ZM scheme in the GATE experiment. It indicates that the proposed triggering function works well not only over middle latitude lands but also over tropical oceans.

Most early studies of cumulus parameterizations used data from tropical measurements (e.g., GATE). There are, however, large differences between tropics and middle latitudes and between ocean and land in terms of the impact of solar diurnal heating. This study has shown that convection triggering function that was developed from tropical data may not be relevant for use over middle latitude lands.

It is noted that perfect simulation results cannot be expected in SCMs due to inevitable uncertainties in observational input data and parameterizations. Yet, a careful analysis could identify the cause of these large simulation biases such as the problem in convection triggering function as shown in this paper. The current study illustrates the possibility of reducing the SCM biases by improving the physical components of the model. Other

approaches have been proposed to specify large-scale forcing terms by using relaxation [*Randall and Cripe*, 1998]. Our work represents an effort to reveal deficiencies of parameterizations that cause the temperature and moisture biases.

It should be also noted that the modifications made in this paper to the convection scheme are only intended to illustrate model deficiencies and possible improvements. The convection triggering condition needs to be further studied in conjunction with more observational data. We also note that any improvements obtained from SCM tests should be transferable to GCMs before the improved parameterizations can be finally implemented onto GCMs. Testing the performance of the proposed convective triggering function in the full CCM3 is being pursued in a separate study.

References

Arakawa, A., and W. H. Schubert, Interaction of a cumulus cloud ensemble with the large-scale environment, Part I, *J. Atmos. Sci*., *31*, 674-701, 1974.

Betts, A. K., and M. J. Miller, A new convective adjustment scheme, Part II: Single column tests using GATE wave, BOMEX, ATEX and arctic air-mass data sets, *Quart. J. Roy. Meteor. Soc*., *112*, 693-709, 1986.

Barnes, S. L., A technique for maximizing details in numerical map analysis, *J. Appl. Meteor*., *3*, 396-409, 1964.

Cripe, D., Single-Column Modeling: sensitivity to initial conditions and divergence forcing, in *Proceedings of the Seventh Atmospheric Radiation Measurement* (ARM), Science Team Meeting, CONF-970365, US Department of Energy, Washington, D. C, 1998.

Emanuel, K. A., Atmospheric Convection, *Oxford University Press,* 580 pp, 1994.

Fritsch, J. M., and J. S. Kain, The Fritsch-Chappell Scheme, The Representation of cumulus convection in numerical models, *a Meteorological Monograph published by the American Meteorological Society,* K. Emanuel and D. Raymond, Eds., 246pp, 1993.

Fritsch, J. M., and C. F. Chappell, Numerical prediction of convectively driven mesoscale pressure systems, Part I: Convective parameterization, *J. Atmos. Sci., 37*, 1722-1733, 1980

Ghan, S., and co-authors: An intercomparison of single column model simulations of summertime midlatitude continental convection, Submitted, 1999.

Grell, G. A., Y.-H, Kuo, and R. Pasch, Semiprognostic tests of cumulus parameterization schemes in the middle latitudes, *Mon. Wea. Rev., 119*, 5-31, 1991.

Hack, J. J., and co-authors, SCCM User's Guide, 1998. (http://www.cgd.ucar.edu/cms/sccm/sccm.html).

Hack, J. J., and J. A. Pedretti, Assessment of solution uncertainties in single-column modeling frameworks, J. Climate, submitted, 1999.

Kain, J. S., and J. M. Fritsch, Convective parameterization for mesoscale models: The Kain-Fritsch scheme, The Representation of Cumulus Convection in Numerical Models, *Meteor. Monogr., No. 46*, Amer. Metero. Soc., 165-170, 1993.

Kiehl, J. T., and co-authors, Description of the NCAR Community Climate Model (CCM3), *NCAR Technical Note, NCAR/TN-420+STR*, 151pp, 1996.

Kuo, H. L., On formation and intensification of tropical cyclones through latent heat release by cumulus convection, *J. Atmos. Sci., 22*, 40-63, 1965.

Kuo, H. L., Further studies of the parameterization of the influence of cumulus convection on large-scale flow, *J. Atmos. Sci., 31*, 1232-1240, 1974.

Kuo, Y.-H., and R. A. Anthes, Semiprognostic tests of Kuo-type cumulus parameterization schemes in an extratropical convective system, *Mon. Wea. Rev., 112*, 1498-1509, 1984.

Lin, X., and R. H. Johnson, Kinematic and thermodynamic characteristics of the flow over thewestern Pacific warm pool during TOGA COARE, *J. Atmos. Sci., 53*, 695-715, 1996.

Lord, S. J., and A. Arakawa, Interaction of a cumulus cloud ensemble with the large-scale environment, Part III: Semiprognostic test of Arakawa-Schubert cumulus parameterization, *J. Atmos. Sci., 39*, 88-103, 1982.

Manabe, S., J. Smagorinsky and R. F. Strickler, Simulated climatology of a general circulation model with a hydrologic cycle, *Mon. Wea. Rev. 93*, 769-798, 1965.

O'Brien, J. J., Alternative solutions to the classical vertical velocity problem, *J. Appl. Meteor., 9*, 197-203, 1970.

Randall, D. A., K-M. Xu, R. J. C. Somerville and S. Iacobellis, Single-column models and cloud ensemble models as links between observations and climate models, *J. Climate, 9*, 1683-1697, 1996.

Randall, D. A., and D. Cripe, Prescribing Advection in Single-Column Models, in *Proceedings of the Seventh Atmospheric Radiation Measurement* (ARM), Science Team Meeting, CONF-970365, US Department of Energy, Washington, D. C, 1998.

Rogers, R., and J. M. Fritsch, A general framework for convective trigger functions, *Mon. Wea. Rev., 124*, 2438-2452, 1996.

Thompson, R. M., Jr., S. W. Payne, E. E. Recker, and R. J. Reed, Structure and properties of synoptic-scale wave disturbances in the intertropical convergence zone of the eastern Atlantic, *J. Atmos. Sci., 36*, 53-72, 1979.

Wang, J., and D. A. Randall, The moist available energy of a conditionally unstable atmosphere, II: Further analysis of the GATE data, *J. Atmos. Sci., 51*, 703-710, 1994.

Wang, J., and D. A. Randall, A cumulus parameterization based on the generalized convective available potential energy, *J. Atmos. Sci., 53*, 716-727, 1996.

Williamson, D. L., The effect of vertical finite difference approximations on simulations with the NCAR Community Climate Model, *J. Climate, 1*, 40-58, 1988.

Williamson, D. L., and P. J. Rasch, Water vapor transport in the NCAR CCM2, *Tellus*, *46A*, 34-51, 1994.

Xu, K.-M., and A.Arakawa, Semi-prognostic tests of the Arakawa-Schubert cumulus parameterization using simulated data, *J. Atmos. Sci., 49*, 2421-2436, 1992.

Yanai, M., S. Esbensen, and J. Chu, Determination of bulk properties of tropical cloud clusters from large-scale heat and moisture budgets, *J. Atmos. Sci., 30*, 611-627, 1973.

Zhang, G. J., and N. A. McFarlane, Sensitivity of climate simulations to the parameterization of cumulus convection in the Canadian Climate Center general circulation model, *Atmosphere-Ocean, 33*, 407-446, 1995.

Zhang, M. H., and J. L. Lin, Constrained variational analysis of sounding data bases on column-integrated budgets of mass, heat, moisture, and momentum: Approach and application to ARM measurements, *J. Atmos. Sci., 54*, 1503-1524, 1997.

Figure Captions

Figure 1. Observations: (a) precipitation rates (mm/day); (b) total advection of temperature (K/day); (c) total advection of moisture (g/kg/day). In (b) and (c), contour interval is 5. Contours greater than 5 or less than -5 are shaded. In these figures, solid lines are for contours greater than or equal to zero and dotted lines for contours less than zero.

Figure 2. Differences between the ensemble mean of simulated temperature and moisture and the observations. (a) Temperature errors (K). (b) Moisture errors (g/kg). (c) Standard deviation of temperature errors (K). For temperature, contour interval is 5 and contours greater than 10 or less than -10 are shaded. For moisture, contour interval is 3 and contours greater than 5 or less than -5 are shaded. For standard deviation, contour interval is o.5. In the figure, solid lines are for contours greater than or equal to zero and dotted lines for contours less than zero.

Figure 3. Time series of the observed (solid line) and ensemble mean of simulated precipitation rates (dotted line) (mm/day). The dash dotted line represents the standard deviations of ensemble mean predicted precipitation.

Figure 4. Time-pressure cross section of the observed and simulated ensemble mean apparent sources Q1 (K/day). Contour interval is 5. Contours greater than 5 are shaded.

Figure 5. Time series of the observed CAPE (J/kg), negative CAPE (NCAPE) (J/kg), and precipitation (mm/day). Solid line is for the CAPE, dashed line for the NCAPE, and dotted line for the precipitation rates.

Figure 6. Relationship between observed dynamic CAPE generation rates (DCAPE) (J/kg/hr, solid line) and precipitation rates (mm/day, dotted line).

Figure 7. Same as Figure 3 except for the ZM_m scheme.

Figure 8. Same as Figure 4b except for the ZM_m scheme.

Figure 9. Same as Figure 2 except for the ZM_m scheme.

Figure 10. Comparison of the simulated (dotted line) and observed (solid line) precipitation rates (mm/day) for the ARM 1997 summer IOP. (a) The ZM scheme. (b) The ZM_m scheme.

Figure 11. Time-pressure cross section of the observed and simulated apparent sources Q1 (K/day) for the ARM 1997 summer IOP. Contour interval is 5. Contours greater than 5 are shade. (a) The ZM scheme. (b) The ZM_m scheme.
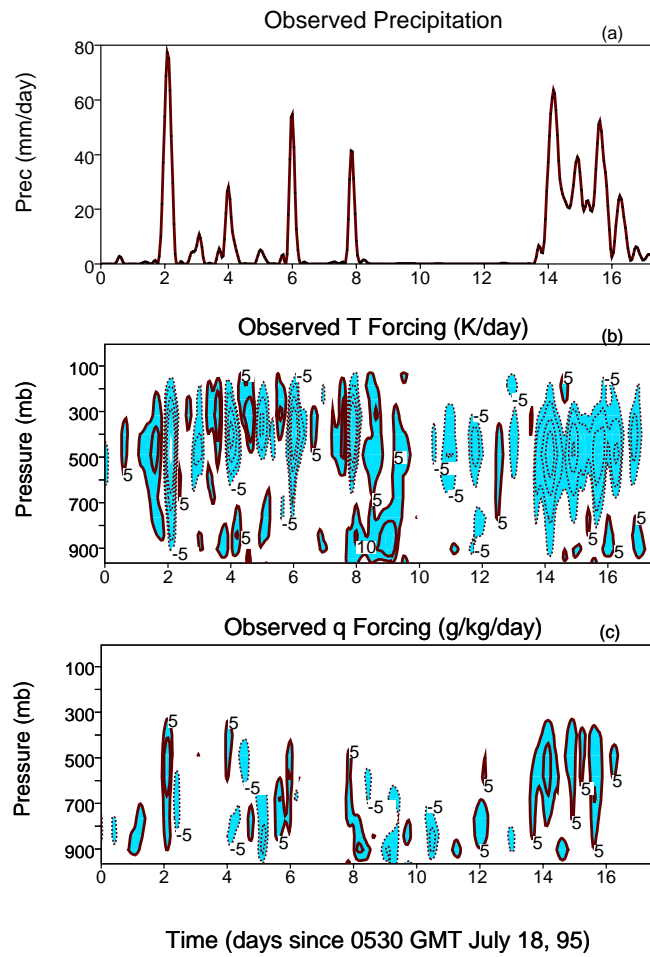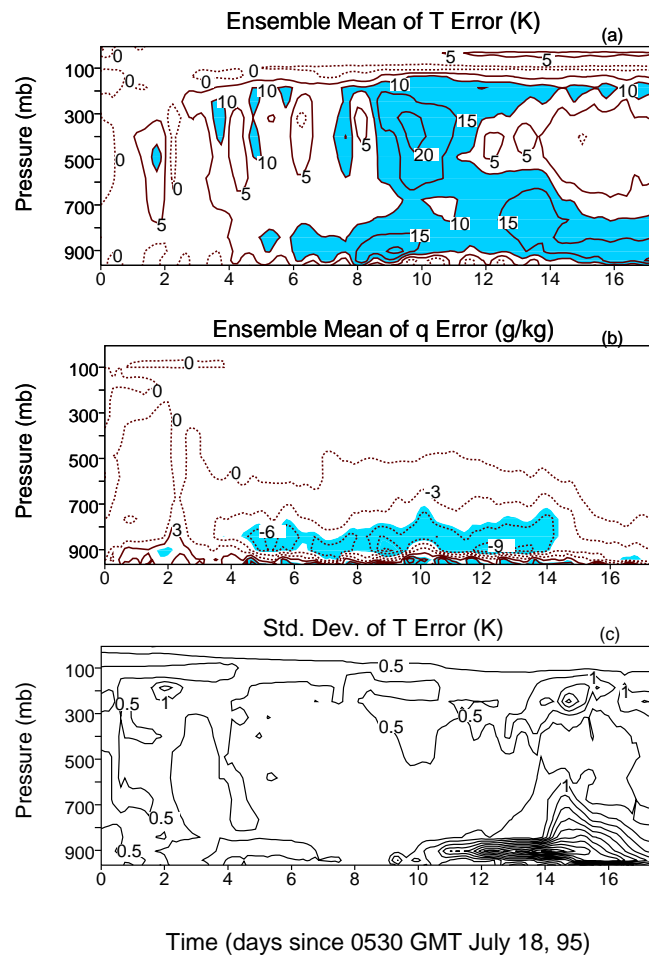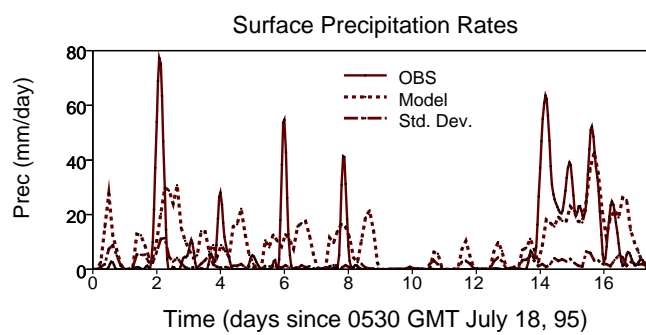
Figure 12. Differences between the simulated and observed temperature (K) for the ARM 1997 summer IOP. Contour interval is 5 and contours greater than 10 or less than -10 are shaded. (a) The ZM scheme. (b) The ZM_m scheme.

Figure 13. Differences between the simulated and observed moisture (g/kg) for the ARM 1997 summer IOP. Contour interval is 3 and contours greater than 5 or less than -5 are shaded. (a) The ZM scheme. (b) The ZM_m scheme.

Figure 14. Comparison of the simulated (dotted line) and observed (solid line) precipitation rates (mm/day) for the GATE experiment. (a) The ZM scheme. (b) The ZM_m scheme.

Figure 15. Time-pressure cross section of the observed and simulated apparent sources Q1 (K/day) for the GATE experiment. Contour interval is 5. Contours greater than 5 are shade. (a) The ZM scheme. (b) The ZM_m scheme.

Figure 16. Differences between the simulated and observed temperature (K) for the GATE experiment. Contour interval is 5 and contours greater than 10 or less than -10 are shaded. (a) The ZM scheme. (b) The ZM_m scheme.

Figure 17. Differences between the simulated and observed moisture (g/kg) for the GATE experimen. Contour interval is 3 and contours greater than 5 or less than -5 are shaded. (a) The ZM scheme. (b) The ZM_m scheme.
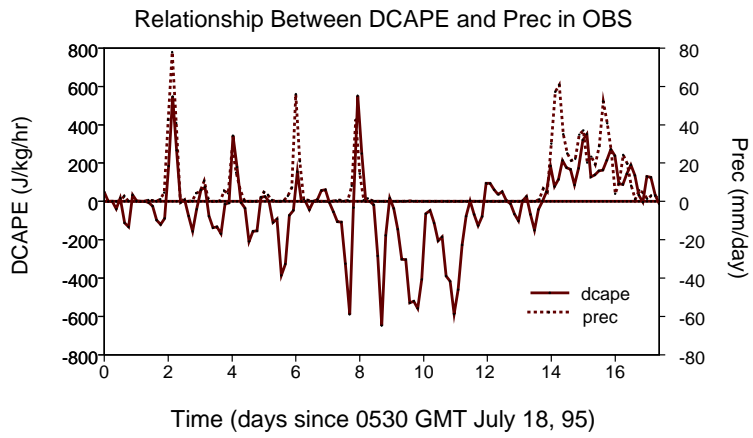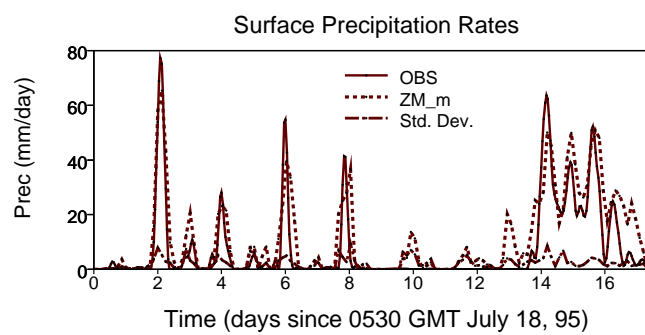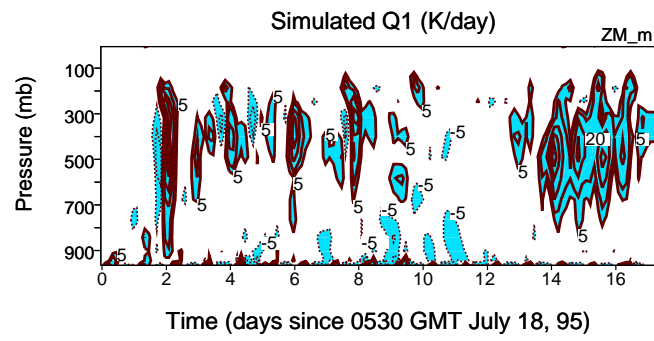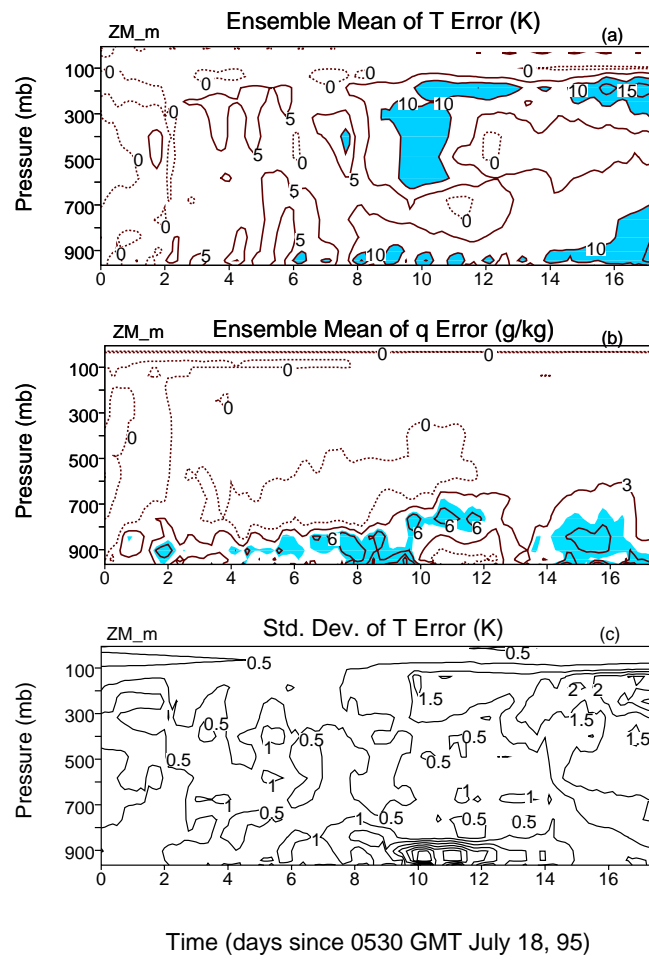
Fig. 1

Fig. 2

Fig. 3
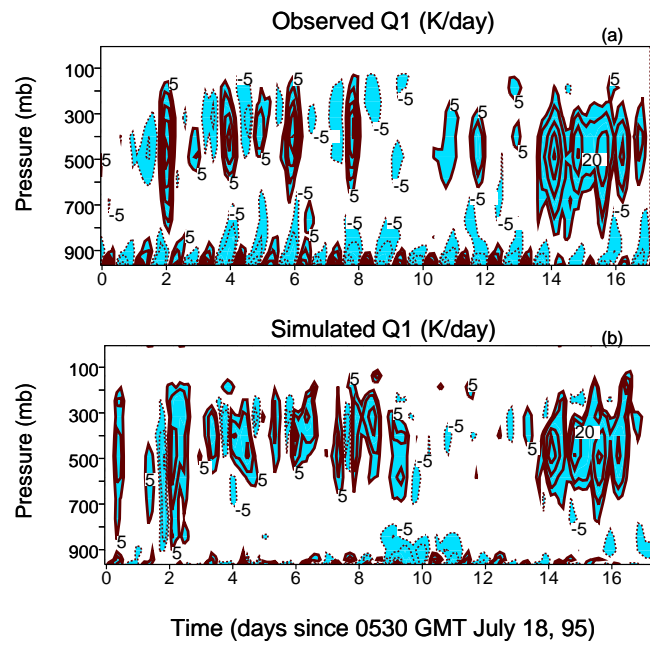
Fig. 4
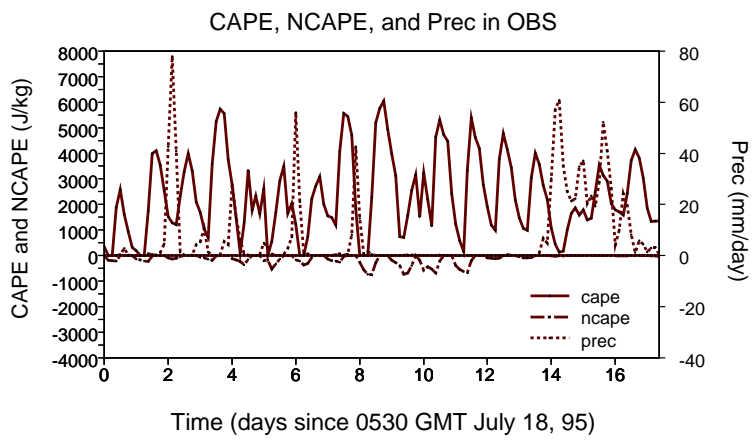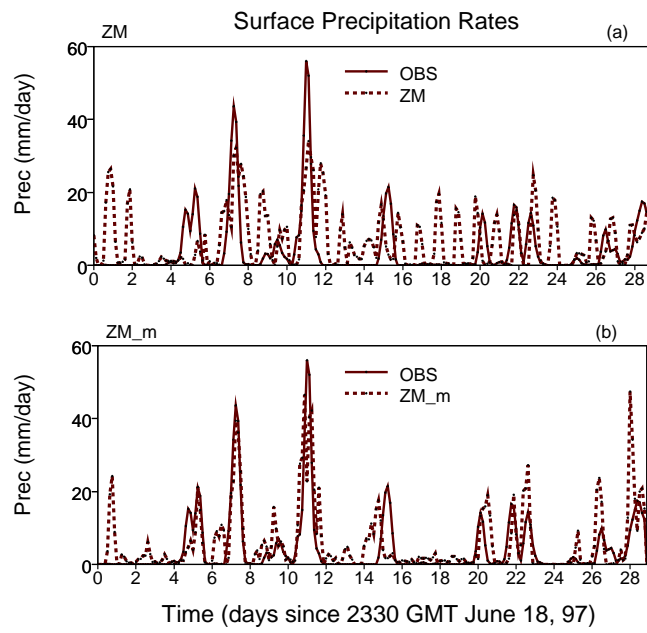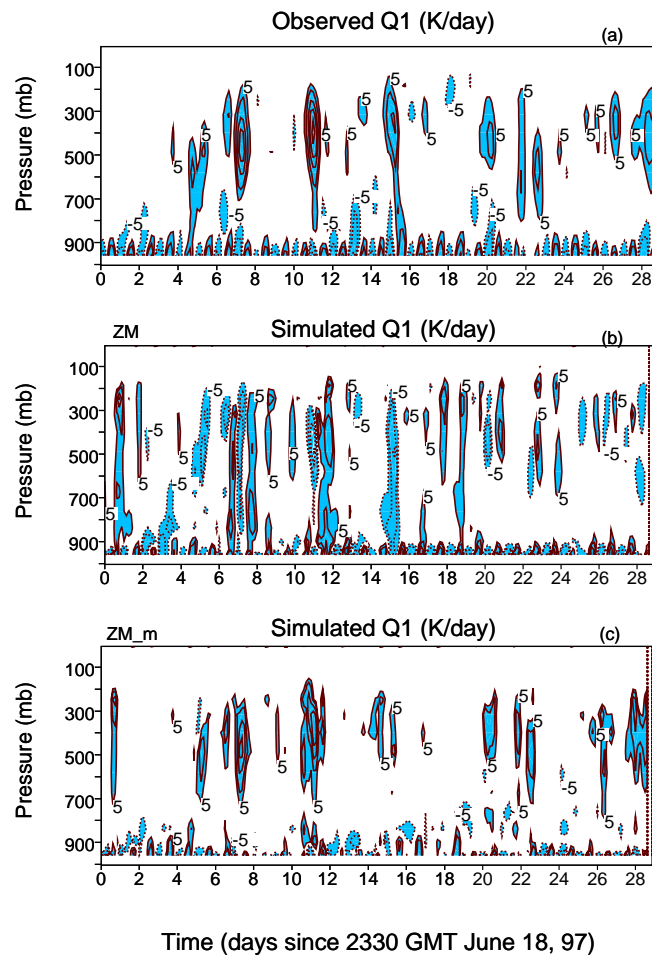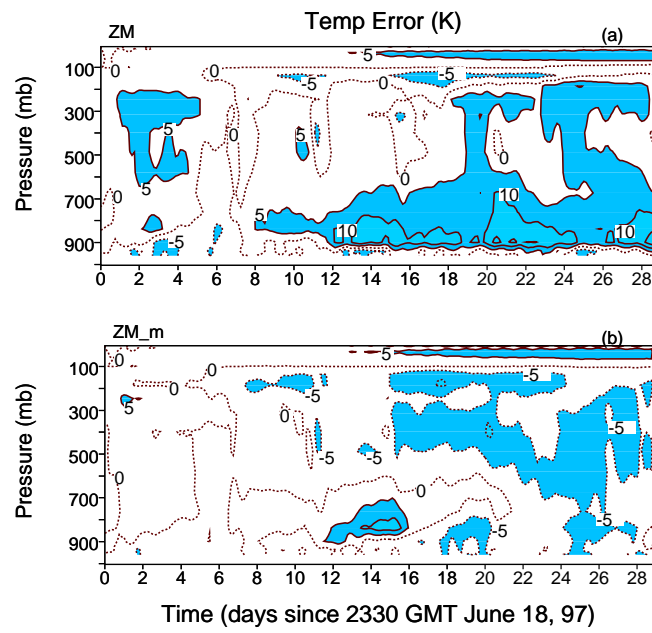
Fig. 5

Fig. 6

Fig. 7

Fig. 8

Fig. 9

Fig. 10

Observed Q1 (K/day) (a)

ZM   Simulated Q1 (K/day) (b)
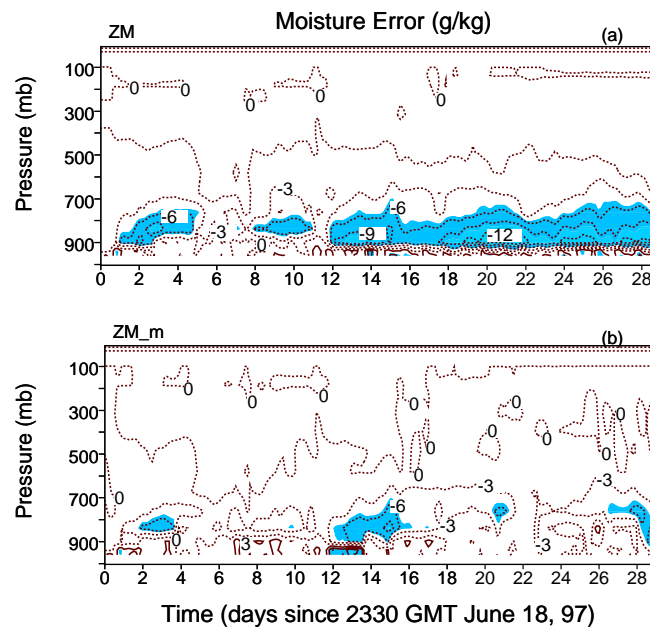
ZM_m   Simulated Q1 (K/day) (c)
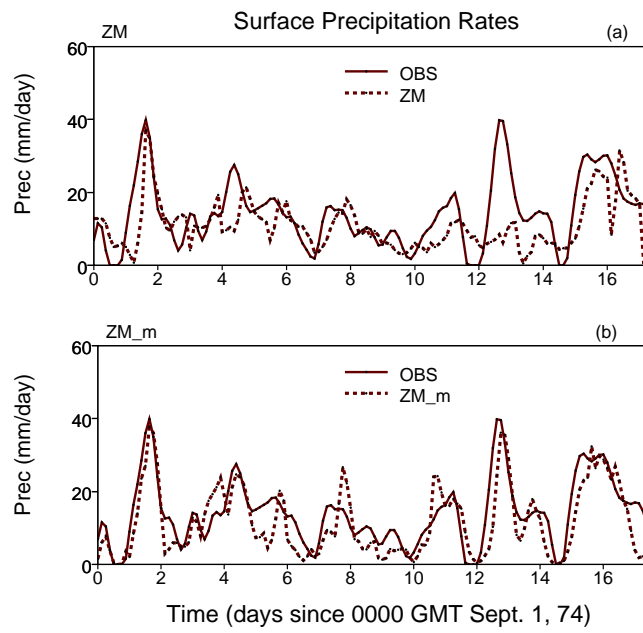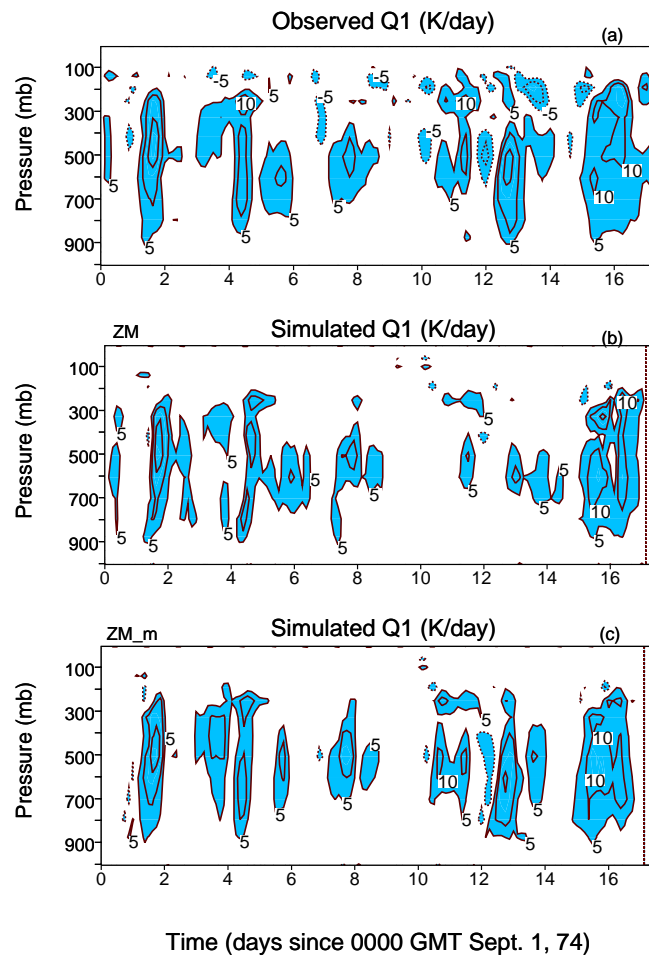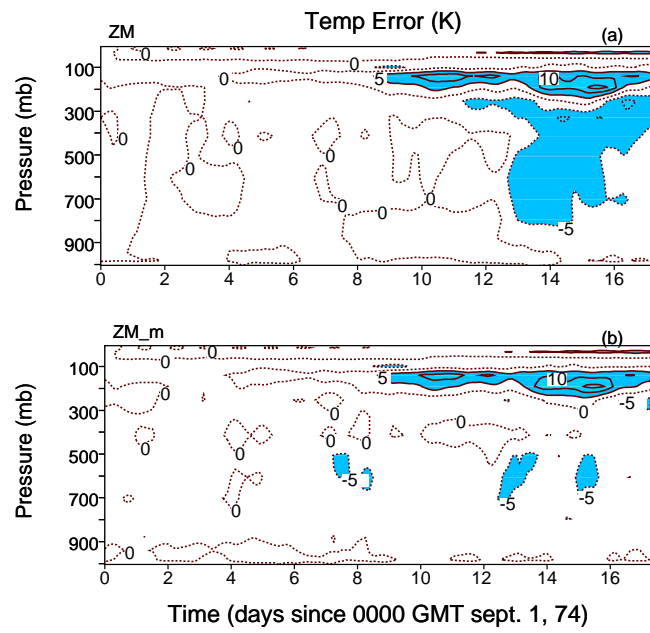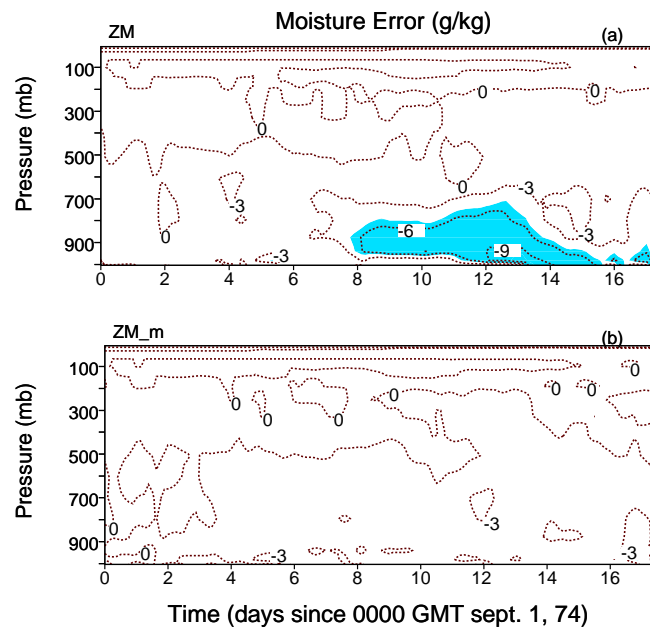
Time (days since 2330 GMT June 18, 97)

Fig. 11

Fig. 12

Fig. 13

Fig. 14

Fig. 15

Fig. 16

Fig. 17